Journal of Advanced Ceramics
2017, **6**(1): 33–42
DOI: 10.1007/s40145-016-0215-z

ISSN 2226-4108
CN 10-1154/TQ

Research Article

Production, characterization, and luminescent properties of Eu^{3+} doped yttrium niobate–tantalate films

Serdar YILDIRIM[a,b,*], Selim DEMIRCI[c], Kadriye ERTEKIN[d], Erdal CELIK[b,e], Zumre Arican ALICIKUS[f]

[a]*The Graduate School of Natural and Applied Sciences, Dokuz Eylul University, Buca, 35390, Izmir, Turkey*
[b]*Center for Fabrication and Applications of Electronic Materials (EMUM), Dokuz Eylul University, Buca, 35390, Izmir, Turkey*
[c]*Department of Metallurgical and Materials Engineering, Marmara University, Goztepe Campus, 34722, Istanbul, Turkey*
[d]*Department of Chemistry, Faculty of Science, Dokuz Eylul University, Buca, 35390, Izmir, Turkey*
[e]*Department of Metallurgical and Materials Engineering, Dokuz Eylul University, Buca, 35390, Izmir, Turkey*
[f]*Department of Radiation Oncology, Dokuz Eylul University, Balcova, 35340, Izmir, Turkey*

Received: October 04, 2016; Revised: October 27, 2016; Accepted: November 19, 2016

Abstract: Monoclinic yttrium tantalate (M′-$YTaO_4$, M′-YTO), and two different kinds of yttrium niobium-tantalate (M′-$YTa_{0.85}Nb_{0.15}O_4$ (M′-YTNO) and Eu^{3+} doped M′-$YTa_{0.85}Nb_{0.15}O_4$ (M′-YTNO:Eu^{3+})) were produced by sol–gel method and grown on single crystalline Si (100) substrate by spin coating approach. Structural properties and thermal behaviours of the films were characterized by means of X-ray diffraction (XRD), atomic force microscopy (AFM), scanning electron microscopy (SEM), and thermogravimetry and differential thermal analysis (TG–DTA). Systematic Steady-state photoluminescence and lifetime measurements in a series of yttrium niobium-tantalate with varying amounts of Eu^{3+} were presented. The photoluminescence spectra of the films exhibited strong blue (380–400 nm) and red (614 nm) emissions upon ultraviolet excitation. Emission intensities were strongly dependent on the host lattice composition and film morphology. 1.5% Eu^{3+} doped films exhibited the brightest luminescence and long lifetime extending to 1.22 ms when excited at 254 nm. To the best of our knowledge, this is the first attempt in the production of M′-YTO, M′-YTNO, and M′-YTNO:Eu^{3+} films on single crystalline Si (100) substrate via sol–gel spin coating.

Keywords: yttrium tantalate; sol–gel; photoluminescence; lifetime; Eu doped

1 Introduction

Development of luminescent materials has been the topic of wide-range research in last decades. Special curiosity has been concentrated on inorganic luminescent materials, which have practical applications in almost all devices involving the artificial production of light [1]. Nowadays, development of field emission displays, flat panels, electroluminescence, scintillators in X-ray, positron emission tomography, and plasma has boosted the request for the luminescent materials with better characteristics in terms of stability, brightness, and

* Corresponding author.
E-mail: serdar.yildirim@deu.edu.tr

industrial processing skills [2].

An X-ray phosphor emits light once it is subjected to X-ray radiation. Yttrium tantalate ($YTaO_4$, YTO) and yttrium niobate ($YNbO_4$, YNO) are efficient as X-ray phosphors utilized in medical imaging. These phosphors which could be used in electronic detector systems and also in films/screen cassettes, fluoroscopy, tomography, and radiography, may also be induced with lower energy sources such as electrons or ultraviolet (UV) light [3–6]. Performances of these phosphors are strongly connected with crystalline structure, composition, particle dimensions, and luminescence behaviours. The blue light emission from yttrium niobium-tantalate $Y(Ta,Nb)O_4$ (YTNO) phosphors under X-ray and UV excitation is incorporated with TaO_4^{3-} and NbO_4^{3-} groups from the host crystalline lattice [7]. YTNO possesses wide and dense absorption bands centered in UV region due to charge transfer (CT) from oxygen to metal, which may potently transfer energy to rare earth activator composing rare earth characteristic emissions [8–10]. Such luminescent emission could be altered toward longer wavelengths when rare earth (RE) ions such as Eu^{3+}, Er^{3+}, Ce^{3+}, Dy^{3+}, Sm^{3+}, and Pr^{3+} are operated to partly substitute yttrium ions in the host lattice. Both host lattice emission and RE emission centers in these phosphors may contribute to the total luminescence. RE activated YTNO type phosphors are good candidates for optoelectronics as much as they have changeable luminescence chromaticity [11].

On the other hand, the RE tantalates and niobates are generally not easy to prepare since they can only be crystallized at temperatures around 1400 ℃. In addition to the difficulty to produce these single phase phosphors, there may be impurity phases in the final product. This is referred in fact that there are generally several yttrium tantalate polymorphs [10,12–14]. To illustrate this, YTO has three crystal structures and presents a complex polymorphism such as high temperature tetragonal (up to 1400 ℃ scheelite, T-structure), low temperature monoclinic (1200–1300 ℃ fergusonite, M-structure), and another monoclinic form called M′ that can be synthesized at lower temperatures. By heating process, M′ phase could transform to T phase, which could transform into M phase during the cooling stage [4]. The two monoclinic crystalline phases including M and M′ exhibit different structural arrangements. In the M′-$YTaO_4$ structure, tantalum atoms are in a distorted octahedral coordination with six Ta–O bonds, whereas in M-$YTaO_4$ tantalum atoms are in tetrahedral coordination. Furthermore, the unit cell volume of M′ phase is approximately half of that of M phase, and the average Ta–O distances are relatively smaller [15–17]. As a result, M′ phase offers more efficient charge transfer process that determines a more intense luminescent emission. The unit cell parameters for M′-$YTaO_4$ are $a = 5.29$ Å, $b = 5.45$ Å, $c = 5.11$ Å, and $\beta = 96.45°$, and the density is 7.57 g/cm^3 [15].

The parameters of the synthesis technique play a key role in controlling the structure and morphology of the phosphors, which determine their optical properties [18,19]. Over the last few years, a number of researches have been carried out on the growth and characterization of luminescent thin films of YTNO. When compared to the powders, thin film phosphors present a few advantages because of their good luminescence characteristics, higher image resolution from small grains, better thermal stability, and good adhesion to the substrate [20–25]. Various chemical and physical methods are utilized for the deposition of luminescent thin films. The deposition of YTNO thin films on single crystalline Si (100) substrate by pulsed laser deposition and metal organic deposition (MOD) was reported earlier [26,27]. Nonetheless, the production of M′-YTO, M′-YTNO, and M′-YTNO: Eu^{3+} films on single crystalline Si (100) substrate via sol–gel spin coating method has not been reported previously. The sol–gel spin coating method is a promising and attractive method on account of good homogeneity, large area coating, and low equipment cost, and provides the opportunity of deposit films on various substrates.

In this study, for the first time, M′-$YTaO_4$, M′-$YTa_{0.85}Nb_{0.15}O_4$, and M′-$Y_{1-x}Eu_xTa_{0.85}Nb_{0.15}O_4$ phosphor films were fabricated on the Si (100) substrates by means of sol–gel spin coating method. The concentration effect of Eu^{3+} on the structure and luminescence properties of the films was also studied in detail. The relationship between the structure and the luminescence performance of the phosphor films was also scrutinized.

2 Experimental studies

2. 1 Preparation of coating solutions and production of phosphor films

$YTaO_4$, $YTa_yNb_zO_4$, and $Y_{1-x}Eu_xTa_yNb_zO_4$ were synthesized by means of sol–gel spin coating technique. All solvents and chemicals, which were received from Sigma Aldrich, were of analytical grade and were used without further purification. Yttrium (III) nitrate hexahydrate ($Y(NO_3)_3{\cdot}6H_2O$, >99%), tantalum (V) ethoxide ($Ta(C_2H_5O)_5$, >99%), niobium (V) ethoxide ($Nb(C_2H_5O)_5$, >99%), and europium (III) nitrate pentahytrate ($Eu(NO_3)_3{\cdot}5H_2O$, >99%) chemicals were utilized as initial precursors. The initial precursors were weighed in convenient quantities in the defined molar ratio and dissolved in absolute ethanol. The quantity of Eu^{3+} doped in $YTa_yNb_zO_4$ ($y=0.85$, $z=0.15$) solution was taken with Y:Eu molar ratios of 0.995:0.005, 0.99:0.01, 0.985:0.015, 0.975:0.025, and 0.95:0.05. First of all, tantalum (V) ethoxide and niobium (V) ethoxide were dissolved in 10 and 5 mL of absolute ethanol respectively, and then solutions were poured together and mixed in order to achieve the molar ratio of Ta:Nb = 0.85:0.15 [28]. Then, yttrium (III) nitrate hexahydrate and europium (III) nitrate pentahydrate solutions were distinctively prepared in 20 and 3 mL of ethanol. Later, the solutions were mixed together so as to obtain the Y:Eu molar ratios of 0.995:0.005, 0.99:0.01, 0.985:0.015, 0.975:0.025, and 0.95:0.05. Solutions were prepared in glove box under nitrogen atmosphere to avoid any oxidation of precursors because of the presenting high sensitivity to humid environment. Amounts of the initial precursors and chemical components to produce phosphor films were listed in Table 1. 3 mL of glacial acetic acid (GAA) was added in all solutions under vigorous stirring for the hydrolysis reaction, where the acetic acid acted as the chelating agent. Before coating, Si (100) substrates were cleaned by an ultrasonic bath in isopropyl alcohol and acetone, respectively, for 30 min each, followed by rinsing with well distilled water and drying in air in order to remove any surface contamination existing on the silicon surfaces. Subsequently, oxygen plasma treatment has been applied during 30 min as the last step in the cleaning process. In the spin coating process, a small drop of the mixed transparent solutions was deposited on or near the center of the cleaned silicon substrates and begun to spin for 40 s at 3000 rpm on both to spread the solutions over the substrates and to wet entire surfaces of the cleaned substrates to obtain films which were further dried at 120 ℃ for 10 min. Spinning and drying cycles were repeated for 5 times. The samples thus were thermally treated in sequences of annealing treatment around at 1200 ℃ for 4 h under ambient atmosphere. Preparation steps for producing films were summarized in Fig. 1.

Table 1 Compositions of the initial precursors

Element	Yttrium	Tantalum	Niobium
Stoichiometric coefficient	1	0.85	0.15
Precursor	Yttrium (III) nitrate hexahydrate	Tantalum (V) ethoxide	Niobium (V) ethoxide
Precursor mass	383.01 g/mol	406.25 g/mol	318.21 g/mol
Mole	0.01	0.01	0.01
Quantity	3.83 g	2.2 mL	0.376 mL
Solvent	Ethanol	Ethanol	Ethanol

2. 2 Characterization

Thermal properties of the samples were characterized with a DTG-60H Shimadzu TG–DTA instrument to determine reaction types of powders and provide convenient process regime in air atmosphere from 25 to 1400 ℃ at a heating rate of 10 ℃/min. Phase identification and crystal structures of samples were performed by means of a Thermo Scientific ARL X-ray diffractometer. This instrument works with voltage and current settings of 45 kV and 44 mA, respectively, and uses Cu Kα radiation (1.5405 Å). For qualitative analysis, XRD diagrams were recorded in the interval $20° \leqslant 2\theta \leqslant 55°$ at a speed of 2 (°)/min. The surface micrographs and topographies of the films

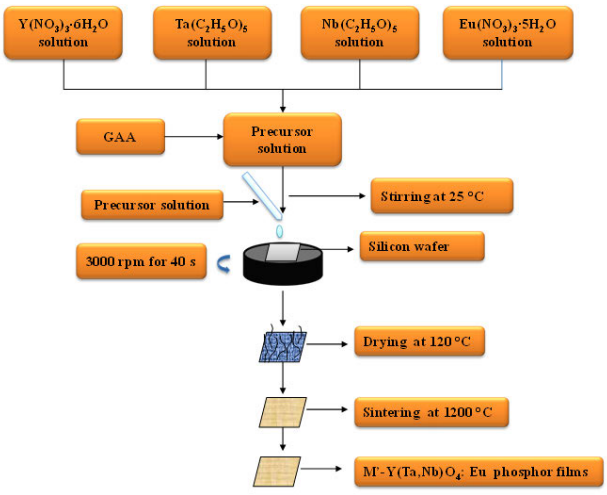

Fig. 1 Diagram of flow chart for production of phosphor films.

were carried out using a JEOL JSM 6060 scanning electron microscope (SEM) and through atomic force microscopy (AFM, EasyScan2, Nanoscience) in contact mode. Steady-state photoluminescence (PL) emission spectra were recorded using a FLS920 spectrofluorometer. Decay time was recorded with a time correlated single photon counting (TCSPC) system that was from Edinburgh Instruments (UK). The instrument was equipped with a standard xenon lamp and a microsecond flash lamp for steady-state and lifetime measurements, respectively. During measurements, the instrument response function (IRF) was obtained from a non-fluorescing suspension of colloidal silica (LUDOX 30%, Sigma Aldrich) in water. The lifetime parameters were recovered by iterative convolution (reconvolution) with a weighted, nonlinear least squares method using the measured IRF and emission decay data. The reduced chi-square values and plots of weighted residuals were used to determine the "goodness of fit" between the calculated and measured decay curves. In all cases, the calculated chi-square values (χ^2) were less than 1.2 and the residual trace symmetrically distributed around the zero axes.

3 Results and discussion

3. 1 Thermogravimetry and differential thermal analysis

To grasp the thermal behaviour of the resulting products and phase transitions during rising temperature in detail, it is necessary to observe TG–DTA curves. DTA and TG curves of $YTaO_4$ xerogel powders are shown in Fig. 2. The TG analysis

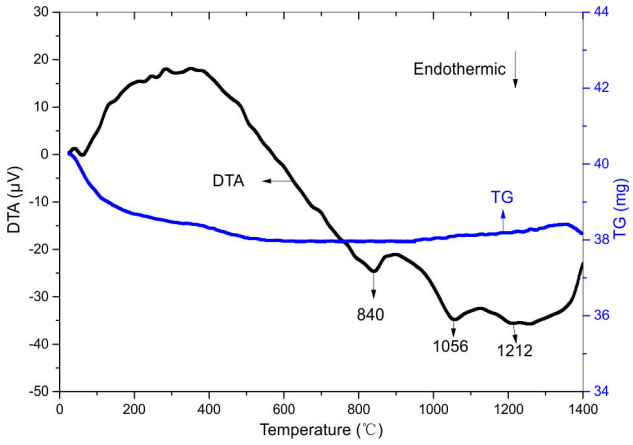

Fig. 2 TG–DTA analysis of $YTaO_4$ xerogel powders.

of the xerogel powders demonstrates that the decomposition of the residuals takes place in two steps. A slight weight loss is registered, which can be attributed to the vaporization of water, accompanying with an endothermic peak at 100 ℃ in the DTA curve in the temperature range of 90–120 ℃. A weight loss peak is observed in the temperature range of 100–450 ℃, corresponding to a broad exothermic peak because of the pyrolysis of the GAA and organic compound on the DTA plot. The weight loss for the two steps is about 2 mg. The endothermic peaks, which can be scrutinized in the DTA plot in the temperature range of 700–1300 ℃, are related to the crystallization, oxidation, and phase transition of the sample. The utilized phosphor exhibits 3 different crystalline structures having different densities through the calcination process. The slight increase observed in the weight after 900 ℃ can be attributed to the formation of new crystalline phases with different structures and densities. Meanwhile, the temperature dependent oxidation and an increase in the mass begin. The applied heat treatment regime is also determined considering these results.

3. 2 XRD crystalline and phase structure

Figure 3 indicates the XRD patterns of M′-YTO, M′-YTNO, and 2.5% Eu^{3+} doped M′-YTNO phosphor films on Si (100) substrates. As can be seen in Fig. 3, the whole phosphor films, which were heated at 1200 ℃ for 4 h in air atmosphere, are well crystallized. The diffraction peaks are in agreement with the monoclinic M′-$YTaO_4$ (JCPDS Card No. 24-1425) phase which belongs to the presence of M′-form of fergusonite structure. All of the other Eu^{3+} doped films exhibit almost the same pattern as 2.5% Eu^{3+} doped M′-YTNO. The substitution of the Nb^{5+} ions in the Ta^{5+} site is theoretically not expected to lead an important distortion since the ionic radii of Nb^{5+} (0.064 nm) and Ta^{5+} (0.065 nm) are almost identical as the coordination number (CN) is 6 [29]. However, a slight shift to higher degrees is observed for the peaks of M′-YTNO as compared to the peaks of M′-YTO. This result is consistent with Ref. [30] which suggests that the decrease of Ta amount can cause shift of main peaks toward higher incident angles. This result may be attributed to the presence of tendency of being off-center of Nb within the octahedral. The shape of the octahedral becomes progressively more distorted at higher Nb content. In addition, Ta leads to more

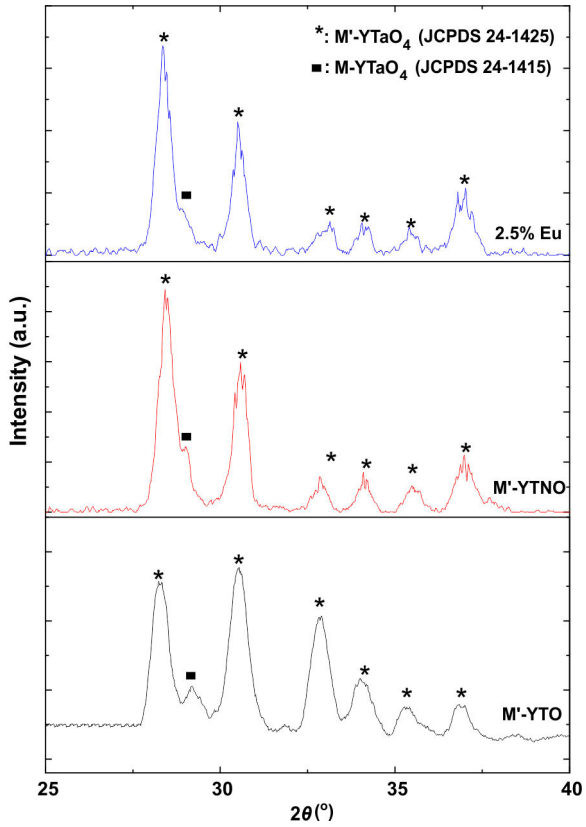

Fig. 3 XRD patterns of M′-YTO, M′-YTNO, and 2.5% M′-YTNO:Eu^{3+} based films onto Si substrates at 1200 ℃ for 4 h in air.

packing in the crystal structure with β tilting distortion [30,31]. Substitution of tantalum ions by up to 15% niobium atoms into the M′-YTO host lattice does not change the basic M′ structure [28]. Low temperature monoclinic (M) phase (JCPDS Card No. 24-1415) is observed as a shoulder at the right side of the 28° peak in all of the films. It can be also observed from Fig. 3 that the main (−111) peak is slightly shifted to lower angles with increasing concentration of Eu^{3+} ions which means the unit cell enlarges because ionic radius of Eu^{3+} (0.950 Å) is slightly larger than that of Y^{3+} (0.893 Å). These results are in good agreement with the crystallographic details of patterns which are analyzed with the Rietveld refinement using the Maud software. The corresponding lattice parameters of all phosphor films from refinement are listed in Table 2. It is seen in Table 2 that the unit volumes of the phosphor films are expanded with increasing Eu^{3+} content. Moreover, the crystalline sizes of the produced films are determined by the Scherrer relation [32] following with $D = k\lambda/\beta\cos\theta$. Here, D is the crystalline size, k is the shape factor which usually takes a value of about

Table 2 Crystallographic details of phosphor films

Compound	*a* (Å)	*b* (Å)	*c* (Å)	*d*-spacing (Å)	Crystalline size (nm)	Unit volume (Å^3)	2θ (°)
M′-YTO	5.31	5.46	5.09	3.1582	34.13	147.57	28.28
M′-YTNO	5.17	5.14	5.00	3.0290	31.56	132.87	29.00
0.5% Eu	5.27	5.49	5.06	3.1422	12.81	146.38	28.50
1.0% Eu	5.30	5.46	5.09	3.1535	15.76	147.29	28.42
1.5% Eu	5.30	5.47	5.09	3.1550	17.81	147.56	28.38
2.5% Eu	5.30	5.46	5.11	3.1561	16.38	147.87	28.36
5.0% Eu	5.39	5.57	5.16	3.1996	18.61	154.92	28.46

0.9, λ is the wavelength of X-ray source used, β is the full width at half-maximum, and θ is the Bragg's diffraction angle. The crystalline sizes of the M′-YTNO:Eu^{3+} phosphors show tendency of increase with the concentration of Eu^{3+}, which are confirmed by findings of the refinement.

3.3 Structure and surface morphology

Figure 4 displays surface morphology of the Eu^{3+} doped films and AFM images of the films with the scale of 3.89 μm × 3.89 μm. Figure 4(a) shows the SEM micrographs of M′-YTNO films. As can be seen from the micrographs, even though the particles do not possess so well-defined morphology, highly dense, well crystallized ellipsoidal and spherical grains are formed without any cracks or pores and exhibit good crystalline quality. Moreover, it is easy to see that the grains of the films become larger and bumpier when Eu^{3+} concentration increases. The study of Marwoto *et al*. [33] confirmed our interpretation that generally the bigger grain configuration with rough surface morphology is observed with increasing of Eu^{3+} content. In our case, the sizes of the grains are in the range of 30–150 nm in diameter. Apart from all these, the SEM inspection shows that the deposited films are quite homogeneous and smooth. Figure 4(b) illustrates the AFM images of phosphor films. To evaluate the surface roughness, an area of 3.89 μm × 3.89 μm was scanned in contact mode. According to the scanning area of the samples, the images for all the films show almost the same topography. Furthermore, it can be observed from the AFM images that the grain size of the M′-YTNO:Eu^{3+} films increases slightly with the increasing amount of Eu^{3+} ions which is consistent with the SEM results. Film roughness is represented by the root mean square (RMS) value. The surface roughness values are found to be between 2 and 5 nm.

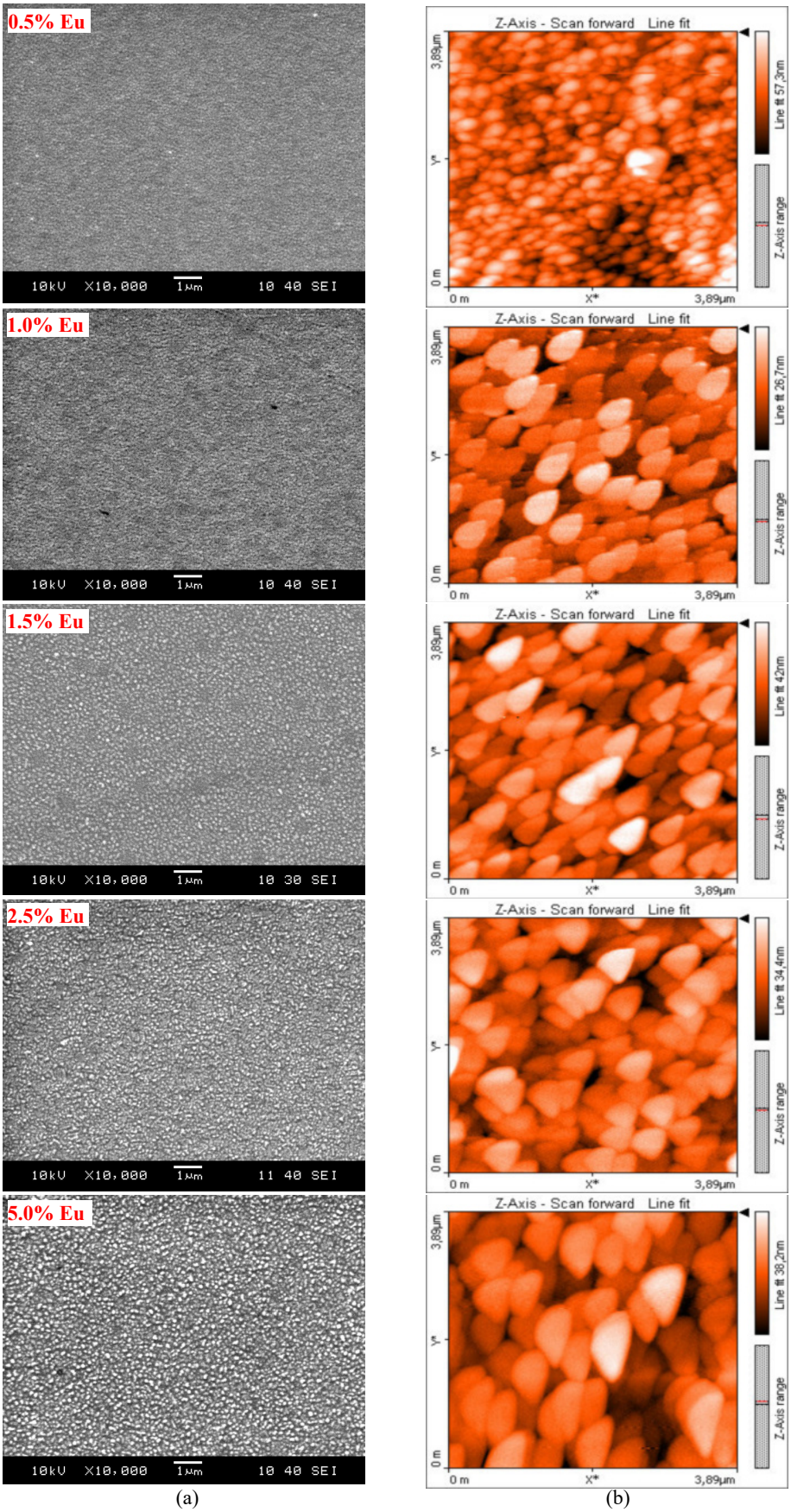

(a) (b)

Fig. 4 (a) SEM and (b) AFM images of M′-YTNO:Eu^{3+} phosphor films.

3. 4 Photoluminescence properties

The luminescent properties of the YTO, YTNO, and Eu^{3+} doped YTNO films grown on Si (100) were determined by photoluminescence spectroscopy. The excitation and emission spectra of the films are shown in Fig. 5. The YTO yields a broad excitation peak at 300 nm arising from charge transfer transitions of TaO_4^{3-}. In Nb doped formulation (YTNO), the excitation maximum exhibits 50 nm of blue shift and appears at 250 nm. In parallel to the excitation spectrum, due to the sensitization effect of Nb ions, the emission maximum of YTNO is observed at 375 and 470 nm exhibiting a distinct red shift with respect to the YTO. The spectral results show that the luminescence of YTO co-doped with Nb and Eu^{3+} is more efficient compared to the single Nb doped YTO (Fig. 5). When this material is co-activated with varying amounts of the Eu^{3+} ions, it exhibits an approximately 10 nm of red shift in the emission maximum and superposed emission characteristics between 375 and 470 nm. Additionally, characteristic red emission band of the Eu centers appears at 614 nm (Fig. 6). The Eu^{3+}-free phosphors do not exhibit emission peak around 600 nm region.

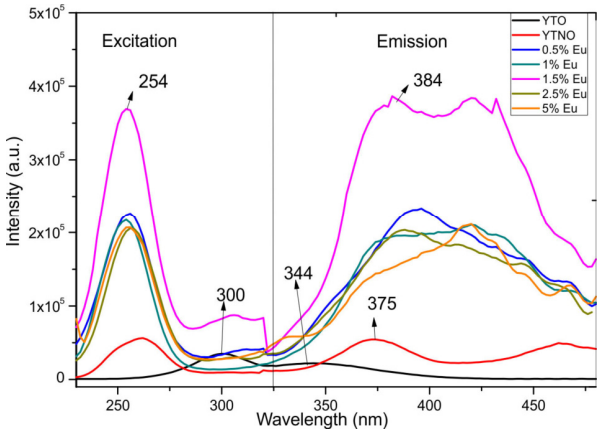

Fig. 5 Excitation and emission spectra of films of YTO, YTNO, and five different concentrations of Eu^{3+} doped yttrium niobium-tantalate.

The intensities arising from the emission of the host around 400 nm peaked at 1.5% Eu^{3+} (Fig. 5). At increasing dopant concentrations, distribution of the Eu^{3+} resulted with pairing and/or coagulation and concentration quenching effects. Yttrium tantalate ($YTaO_4$) phosphor is an ultraviolet emitter (λ_{em} = 344 nm) whose luminescence corresponds to a charge transfer transition including TaO_4^{3-} groups. When Nb ions are partially (15%) substituted for Ta ions in M′-$YTaO_4$ structure, NbO_4^{3-} centers are formed that generate a blue-shifted luminescence emission between 375 and 450 nm [34]. As shown in the literature, under 254 nm excitation, only the niobate group but not the host lattice is excited [35].

Further emission spectra and corresponding transitions of Eu^{3+} ($^5D \rightarrow {}^7F_j$ (j = 1, 2, 3, and 4)) are shown in Fig. 6. When rare earth ions such as Eu^{3+} are meanwhile included partly subrogating the Y^{3+} ions from the host crystalline lattice, Eu^{3+} emission centers are composed. In this instance, the excitation energy is firstly absorbed by the host lattice [36]. The absorbed energy may then be transferred to TaO_4^{3-} or NbO_4^{3-} groups and at last, transferred to the Eu^{3+} centers.

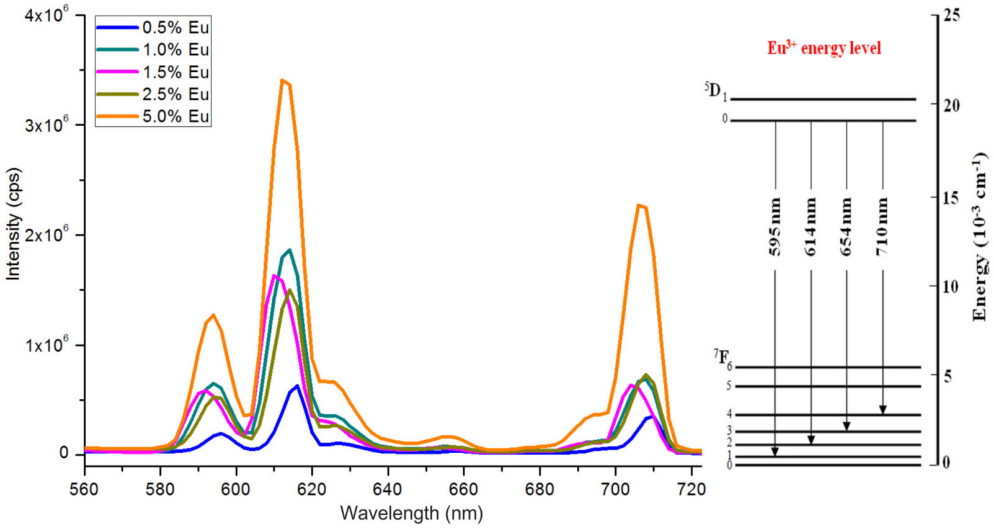

Fig. 6 Emission spectra and corresponding transition bands of Eu^{3+} doped films.

Europium is widely known that the luminescence originating from transitions between 4f levels is mainly owing to electric dipole coactions [37].

Here the specific red emission band of Eu that is situated at 614 nm is due to electronic transition of $^5D_0 \rightarrow {}^7F_2$ of inside Eu^{3+} ion with 4f configurations (Fig. 6). The PL spectra also show the well known emission lines arising from $^5D_0 \rightarrow {}^7F_1$ (595 nm), $^5D_0 \rightarrow {}^7F_3$ (654 nm), and $^5D_0 \rightarrow {}^7F_4$ (710 nm) transitions of Eu^{3+}. The luminescent emission centers are red shifted towards longer wavelengths, and both luminescent centers conduced to the whole luminescence.

3. 5 Decay time measurements

The films of YTO, YTNO, and YTNO:Eu^{3+} were excited with a microsecond flash lamb at 300, 262, and 254 nm, respectively (Table 3). Decay curves of the films were recorded at two different emission maxima, around 400 and 614 nm, respectively. While the data acquired around 400 nm are arising from the transitions of the host and synthesizers, the data acquired at the red region can be assigned to characteristic transitions of Eu^{3+}. We have studied around 400 nm spectral range to be able to compare the emission characteristics of the all phosphors. The decay data acquired around 400 nm were monitored after the excitation deduction, and on the principle of the exponential formula, the decay time was determined, i.e., the time after which the intensity is dropped to 1/e from the initial value:

$$I(t) = Ae^{(-t/\tau_1)} + Be^{(-t/\tau_2)} + Ce^{(-t/\tau_3)} \quad (1)$$

The curves were fitted with a third order exponential (Eq. (1)), where I is the luminescence intensity, A, B, and C are constants, and t is the time. Figure 7(a) reveals the average fluorescence lifetime recorded for films of Eu^{3+}-free host and for five different concentrations of Eu^{3+} doped YTNO around 400 nm. Table 3 reveals lifetime related data of the studied structures in detail. When the emission was monitored at 400 nm, the composites exhibited multi-exponential decays. The shortest lifetime components were appeared between 18 and 69 μs for the studied formulations. The average longer and longest lifetime were reported around 300 and 1800 μs, respectively. Contribution of the longer and longest lifetime components to mean lifetime was dominant and was at an average of 40% and 50% for the mid and the last, respectively. The observed three exponential decay time in films can be attributed to the structural properties of the host matrix and formation of three different microenvironments for the rare earth dopant. Presence of the europium ions in the host caused an enhancement in the decay time up to 1.5% Eu^{3+}. However, after that critical concentration of the europium, the decay time data acquired at 400 nm were shortened. When the spectral patterns and results of the lifetime measurements were evaluated together, it can be concluded that the 1.5% Eu^{3+} is optimum. The decay dynamics acquired at 614 nm were different from the ones observed at 400 nm in terms of the slopes of the decay curves (Fig. 7(b)). While the 400 nm region exhibited three exponential quenching, the decays observed at 614 nm were mono-exponential. However, the average decay time acquired at both regions was in accordance with each other (Table 3).

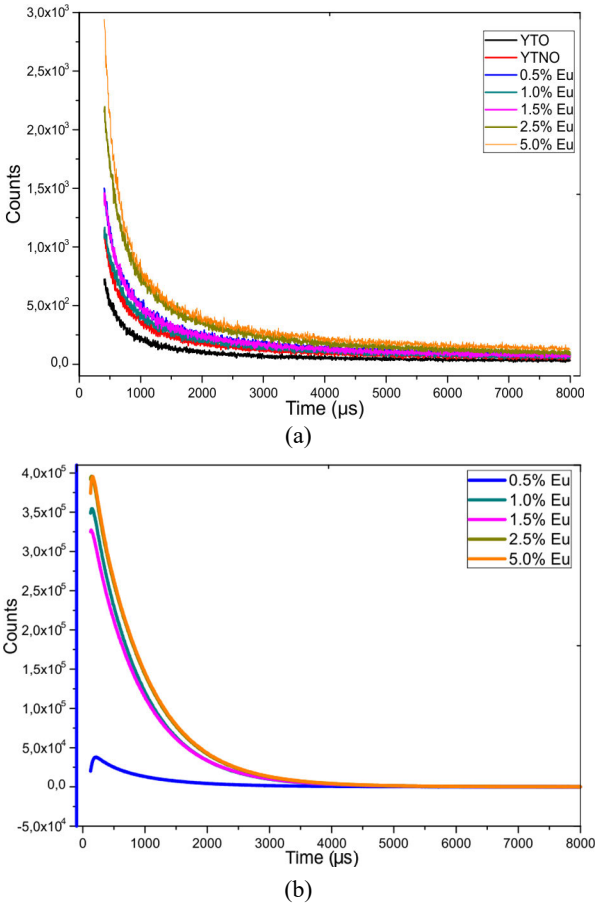

Fig. 7 Decay curves of YTO, YTNO, and YTNO:Eu^{3+} doped films as a function of doping concentration acquired at two different wavelengths: (a) 350–400 nm, (b) 614 nm.

Table 3 Fluorescence lifetime of films of Eu^{3+}-free host and five different concentrations of Eu^{3+} doped YTNO composites

Sample	λ_{max}^{ex} , λ_{max}^{em} (nm)	χ^2		Decay time (μs)	Standart dev. (μs)	Rel. (%)	λ_{max}^{em} (614 nm)
M′-YTO	300, 344	1.192	τ_1	25.90	0.75	9.41	—
			τ_2	221.82	3.29	42.17	
			τ_3	1519.64	26.08	48.42	
			τ_{avr}		831.79 μs		
M′-YTNO	262, 374	1.199	τ_1	27.48	0.67	9.19	—
			τ_2	239.52	3.98	33.15	
			τ_3	1624.78	23.62	57.66	
			τ_{avr}		1018.78 μs		
0.5% Eu	254, 396	1.176	τ_1	50.49	1.44	8.56	τ_1 = 737 μs
			τ_2	319.31	6.15	34.70	
			τ_3	1932.85	37.39	56.74	
			τ_{avr}		1211.82 μs		
1.0% Eu	254, 400	1.111	τ_1	18.23	0.36	7.75	τ_1 = 970 μs
			τ_2	263.31	3.55	33.78	
			τ_3	1927.93	25.01	58.46	
			τ_{avr}		1217.43 μs		
1.5% Eu	254, 388	1.175	τ_1	69.54	2.60	9.47	τ_1 = 1012 μs
			τ_2	333.57	8.39	33.91	
			τ_3	1947.85	40.47	56.63	
			τ_{avr}		1222.77 μs		
2.5% Eu	254, 387	1.192	τ_1	27.61	0.70	5.25	τ_1 = 1024 μs
			τ_2	293.22	3.24	37.36	
			τ_3	1782.51	22.28	57.40	
			τ_{avr}		1134.16 μs		
5.0% Eu	254, 396	1.199	τ_1	38.67	0.36	19.23	τ_1 = 1032 μs
			τ_2	282.32	3.53	33.21	
			τ_3	1800.26	25.12	47.56	
			τ_{avr}		957.40 μs		

4 Conclusions

In summary, YTO, YTNO, and YTNO:Eu^{3+} phosphors which are used in films/screen cassettes, electronic detector systems, and computed tomography and fluoroscopy were fabricated by sol–gel spin coating method for the first time. The surface morphologies of the films became larger and bumpier when Eu^{3+} concentration increased. Effect of varying amounts of Eu^{3+} concentration on spectral properties has been followed by steady-state photoluminescence and lifetime measurements. The PL spectra of YTNO:Eu^{3+} exhibited broad and intense emission bands around 400 nm and the well known emission lines arising from $^5D_0 \rightarrow {}^7F_1$ (595 nm), $^5D_0 \rightarrow {}^7F_2$ (614 nm), $^5D_0 \rightarrow {}^7F_3$ (654 nm), and $^5D_0 \rightarrow {}^7F_4$ (710 nm) transitions of Eu^{3+} when excited with the UV radiation. One of the most potential applications of the offered phosphor is the scintillating process which requires short wavelength excitation and light conversion to longer wavelengths. Here we accomplished to convert the UV excitation light at 254 nm to visible (380–450 nm) and further red light (614 nm). Additionally, the RE dopant (Eu^{3+}) provided enhanced luminescence intensity with respect to the RE-free formulations. The best lifetime value and highest luminescence intensity were obtained for 1.5% Eu^{3+} doped film as 1.22 ms at emission wavelength of 388 nm.

Acknowledgements

This research was fully supported by Scientific and Technical Research Council of Turkey (TUBITAK) under Project No. SBAG-113S069.

References

[1] Pereira PFS, Matos MG, Ávila LR, *et al*. Red, green and blue (RGB) emission doped $Y_3Al_5O_{12}$ (YAG) phosphors prepared by non-hydrolytic sol–gel route. *J Lumin* 2010, **130**: 488–493.

[2] Huang H, Yan B. *In situ* sol–gel composition of multicomponent hybrid precursor to hexagon-like Zn_2SiO_4:Tb^{3+} microcrystalline phosphors with different silicate sources. *Appl Surf Sci* 2006, **252**: 2967–2972.

[3] Blasse G, Grabmaier BC. *Luminescent Materials*. Springer Berlin Heidelberg, 1994.

[4] Brixner LH. New X-ray phosphors. *Mater Chem Phys* 1987, **16**: 253–281.

[5] Sonoda M, Takano M, Miyahara J, *et al*. Computed

radiography utilizing scanning laser stimulated luminescence. *Radiology* 1983, **148**: 833–838.
[6] Curry TS, Dowdey JE, Murry RC. *Christensen's Physics of Diagnostic Radiology*. Lippincott Williams & Wilkins, 1990.
[7] Blasse G, Bril A. Photoluminescent efficiency of phosphors with electronic transitions in localized centers. *J Electrochem Soc* 1968, **115**: 1067–1075.
[8] Maschio S, Bachiorrini A, Di Monte R, *et al*. Preparation and characterization of $LaNbO_4$ from amorphous precursors. *J Mater Sci* 1995, **30**: 5433–5437.
[9] Issler SL, Torardi CC. Solid state chemistry and luminescence of X-ray phosphors. *J Alloys Compd* 1995, **229**: 54–65.
[10] Gu M, Xu X, Liu X, *et al*. Preparation and characterization of $GdTaO_4$:Eu^{3+} sol–gel luminescence thin films. *J Sol–Gel Sci Technol* 2005, **35**: 193–196.
[11] Ayvacıklı M, Ege A, Ekdal E, *et al*. Radioluminescence study of rare earth doped some yttrium based phosphors. *Opt Mater* 2012, **34**: 1958–1961.
[12] Popovici E-J, Nazarov M, Muresan L, *et al*. Synthesis and characterisation of terbium activated yttrium tantalate phosphor. *J Alloys Compd* 2010, **497**: 201–209.
[13] Maillard P, Tessier F, Orhan E, *et al*. Thermal ammonolysis study of the rare-earth tantalates $RTaO_4$. *Chem Mater* 2005, **17**: 152–156.
[14] Gasparotto G, Nascimento NM, Cebim MA, *et al*. Effect of heat treatment on the generation of structural defects in $LaTaO_4$ ceramics and their correlation with photoluminescent properties. *J Alloys Compd* 2011, **509**: 9076–9078.
[15] Brixner LH, Chen H-y. On the structural and luminescent properties of the M′ $LnTaO_4$ rare earth tantalates. *J Electrochem Soc* 1983, **130**: 2435–2443.
[16] Weitzel H, Schröcke H. Kristallstrukturverfeinerungen von Euxenit, $Y(Nb_{0.5}Ti_{0.5})_2O_6$, und M-Fergusonit, $YNbG_4$. *Zeitschrift für Kristallographie* 1980, **152**: 69–82.
[17] Jehng JM, Wachs IE. Structural chemistry and Raman spectra of niobium oxides. *Chem Mater* 1991, **3**: 100–107.
[18] Karsu EC, Popovici EJ, Ege A, *et al*. Luminescence study of some yttrium tantalate-based phosphors. *J Lumin* 2011, **131**: 1052–1057.
[19] Arellano I, Nazarov M, Byeon CC, *et al*. Luminescence and structural properties of $Y(Ta,Nb)O_4$:Eu^{3+},Tb^{3+} phosphors. *Mater Chem Phys* 2010, **119**: 48–51.
[20] Hirata GA, McKittrick J, Avalos-Borja M, *et al*. Physical properties of Y_2O_3:Eu luminescent films grown by MOCVD and laser ablation. *Appl Surf Sci* 1997, **113–114**: 509–514.
[21] Bae JS, Moon BK, Choi BC, *et al*. Photoluminescence behaviors in $ZnGa_2O_4$ thin film phosphors deposited by a pulsed laser ablation. *Thin Solid Films* 2003, **424**: 291–295.
[22] Gonzalez-Ortega JA, Tejeda EM, Perea N, *et al*. White light emission from rare earth activated yttrium silicate nanocrystalline powders and thin films. *Opt Mater* 2005, **27**: 1221–1227.
[23] Bae JS, Kim SB, Jeong JH, *et al*. Photoluminescence characteristics of Li-doped Y_2O_3:Eu^{3+} thin film phosphors. *Thin Solid Films* 2005, **471**: 224–229.
[24] Bae JS, Shim KS, Kim SB, *et al*. Photoluminescence characteristics of pulsed laser deposited $Y_{2-x}Gd_xO_3$:Eu^{3+} thin film phosphors. *J Cryst Growth* 2004, **264**: 290–296.
[25] Kim SS, Moon JH, Lee B-T, *et al*. Microstructures of pulsed laser deposited Eu doped Y_2O_3 luminescent films on Si (001) substrates. *Appl Surf Sci* 2004, **221**: 231–236.
[26] Mesaros A, Nasui M, Petrisor Jr. T, *et al*. Synthesis of $YTaO_4$:Nb thin films by chemical solution deposition. *J Alloys Compd* 2012, **543**: 221–226.
[27] Mesaros-Hristea A, Alm O, Popovici E-J, *et al*. Luminescent thin films of nanocrystalline $YTaO_4$:Nb by pulsed laser deposition. *Thin Solid Films* 2008, **516**: 8431–8435.
[28] Hristea A, Popovici E-J, Muresan L, *et al*. Morpho-structural and luminescent investigations of niobium activated yttrium tantalate powders. *J Alloys Compd* 2009, **471**: 524–529.
[29] Shannon RD. Revised effective ionic radii and systematic studies of interatomic distances in halides and chalcogenides. *Acta Cryst* 1976, **A32**: 751–767.
[30] Lee CW, Park HK, Park S, *et al*. Ta-substituted $SnNb_{2-x}Ta_xO_6$ photocatalysts for hydrogen evolution under visible light irradiation. *J Mater Chem A* 2015, **3**: 825–831.
[31] Wetherall KM, Doughty P, Mountjoy G, *et al*. The atomic structure of niobium and tantalum containing borophosphate glasses. *J Phys: Condens Matter* 2009, **21**: 375106.
[32] Demirci S, Öztürk B, Yildirim S, *et al*. Synthesis and comparison of the photocatalytic activities of flame spray pyrolysis and sol–gel derived magnesium oxide nano-scale particles. *Mat Sci Semicon Proc* 2015, **34**: 154–161.
[33] Marwoto P, Sugianto S, Wibowo E. Growth of europium-doped gallium oxide (Ga_2O_3:Eu) thin films deposited by homemade DC magnetron sputtering. *J Theor Appl Phys* 2012, **6**: 17.
[34] Hristea A, Popovici EJ, Muresan L, *et al*. Yttrium-tantalate-based phosphors for X-ray intensifying screen. In Proceedings of ROMOPTO 2003: Seventh Conference on Optics. International Society for Optics and Photonics, 2004: 781–787.
[35] Blasse G, Bril A. Luminescence phenomena in compounds with fergusonite structure. *J Lumin* 1970, **3**: 109–131.
[36] Nazarov M. *New Generation of Europium-and Terbium-Activated Phosphors: From Syntheses to Applications*. CRC Press, 2011.
[37] Nazarov MV, Zamoryanskaya MV, Popovici E-J, *et al*. Luminescence of calcium tungstate phosphors doped with europium and terbium. *J Mold Phys Sci* 2003, **2**: 68–79.